DEM Simulation of a Bio-Inspired Self-Burrowing Probe in Granular Materials

Ningning Zhang, Ph.D.¹; Yuyan Chen, Ph.D.²; Alejandro Martinez, Ph.D., A.M.ASCE³; and Raul Fuentes, Ph.D.⁴

¹Institute of Geomechanics and Underground Technology, RWTH Aachen Univ., Aachen,

Germany. Email: n.zhang@gut.rwth-aachen.de

²Dept. of Civil and Environmental Engineering, Univ. of California, Davis, CA.

Email: yych@ucdavis.edu

³Dept. of Civil and Environmental Engineering, Univ. of California, Davis, CA.

Email: amart@ucdavis.edu

⁴Institute of Geomechanics and Underground Technology, RWTH Aachen Univ., Aachen,

Germany. Email: raul.fuentes@gut.rwth-aachen.de

ABSTRACT

Traditional soil penetration activities such as site investigation and pile driving are energyintensive and typically cause significant disturbance to surrounding soils and the environment. In recent years, researchers have attempted to solve the abovementioned problems by developing self-burrowing tools and probes on the basis of biological inspiration. Animals such as razor clams are capable of efficiently burrowing into soils using a dual-anchor mechanism, which cyclically alternates penetrating the back (shell) and front (foot) anchors to achieve forward movement. Due to inherent complexities of the self-burrowing mechanism, the interaction between a clam-inspired probe and soil is not fully understood yet. This study employs models based on the discrete element method (DEM) to investigate this soil-structure interaction problem. The soil sample is filled with a scaled discrete quartz sand analogue. The selfburrowing behavior of the probe is fully modeled using force-control motion, which enables realistic interaction with the surrounding soil. The strategy of tip oscillation is also employed to reduce soil penetration resistance. The simulation results show that the self-burrowing probe can achieve significant advancement, especially when tip oscillation is used. Micromechanical observations such as contact force networks and displacement fields are also provided to better understand the interaction between the soil and the bio-inspired probe. This study provides meaningful guidance for future self-burrowing probe development.

INTRODUCTION

Conventional geotechnical activities such as pile installation, in-situ testing, and cable installation generally require high energy consumption and typically cause ground disturbance. The development of probes inspired by animals and plants (i.e., bio-inspired) can help reduce environmental and energetic impacts of soil penetration activities due to their increased energy efficiency and the fact that drill rigs do may need to be mobilized to the site (Chen et al., 2021; Martinez et al., 2021). Self-burrowing technologies could also help reduce the size of the equipment required for subsurface exploration, thus facilitating access to limited-access areas in project sites as well as in other planets and asteroids in the solar system.

To develop bio-inspired technologies for geotechnical practice, some particular burrowing species such as the razor clams (Trueman, 1967), caecilians, and earthworms can be chosen for

inspiration. Razor clams, which are capable of efficiently burrowing into sands using a dual-anchor mechanism, have attracted great attention due to their prominent efficiency and the simplicity of their burrowing strategy. They cyclically alternate expansion and contraction of their back (shell) and front (foot) anchors to achieve forward movement (Trueman, 1967). During a cycle, the shell is first expanded to form an anchor to provide sufficient reaction force for the foot can penetrate further into the soil. Then, the foot is expanded and the shell is contracted. In this stage, the foot acts as an anchor to drag the shell down into the soil.

In recent years, researchers have performed investigations on self-burrowing probes by means of various methods. For instance, Winter et al. (2014) developed a razor clam-inspired probe called 'RoboClam' and Martinez et al. (2020) used cavity expansion theory to assess self-penetration potential in various soils. DEM models have been extensively used in self-burrowing studies due to their advantages in providing both macroscopic and particle-scale results. Chen et al. (2021) performed DEM simulations of a self-penetration probe for in-situ testing, while Huang & Tao (2020) presented DEM results of simulations of a razor clam-inspired probe. These DEM studies could help further understand the soil-probe interactions. However, studies to date have considered probes with only one deployable anchor, resembling the configuration of cone-pressuremeter probe. In the present study, we use DEM to model a dual-anchor self-burrowing probe and test its behavior in granular materials.

MODEL CONSTRUCTION

In this study, we use the DEM code PFC3D (Itasca, 2017) to create a discrete analogue mimicking the mechanical properties of Fontainebleau sand, which has been extensively used in geotechnical research. Particle diameters ranged from 0.1 to 0.4 mm matching the particle size distribution of Fontainebleau NE34 sand (Figure 1a). Particle rotation was not allowed in order to approximate the interlocking effect of non-spherical particles (Ting et al., 1989). The contact model developed by Zhang et al. (2021) for rough crushable particles was chosen to numerically reflect Fontainebleau sand behaviour in a more realistic way. The model was developed based on the standard Hertzian model with the following characteristics: contacts between particles are assumed to be elastoplastic, the slip behavior at contacts is defined by a friction coefficient μ , and each contact has a non-linear stiffness controlled by the elastic properties of material particles (e.g., shear modulus, G, and Poisson's ratio, v). This model is also able to consider more realistic soil characteristics by incorporating the effects of the particle surface roughness, S_q , and particle crushing in the standard Hertzian model. The modeling parameters used in this study are presented in Table 1 and details on the calibration of these parameters can be found in Zhang et al. (2021). The particle crushing algorithm was not considered in this study due to the relatively low stress level encountered during penetration.

A three-dimensional cylindrical chamber was constructed using frictionless wall elements. Geometrical model details can be found in Figure 1b and Table 2. The particle sizes were upscaled applying five distinct scaling factors following the particle refinement method (PRM) (Ciantia et al., 2018; Huang & Tao, 2020; McDowell et al., 2012; Sharif et al., 2020). This method allows to increase the number of contacts between the particles and probe in a computationally efficient way to ensure numerical stability. The upscaling of particle sizes does not limit the precision of the overall response as particle mechanical properties remain unchanged (McDowell et al., 2012).

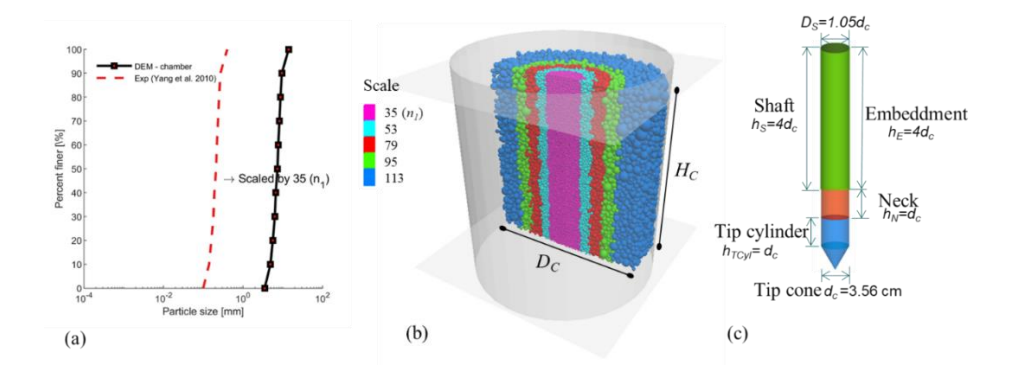


Figure 1. (a) Particle size distribution of Fontainebleau sand, (b) view of DEM model with multi-scaled particles, and (c) view of bio-inspired dual-anchor probe prototype

Table 1. DEM contact model parameters

Element	G (GPa)	v	μ	$S_{q}(\mu m)$	n ₁ *	n2*
F-sand	2.5	0.19	0.275	0.6	0.05	5
Probe	3.75	0.265	0.35	-	_	-

^{*} n_1 and n_2 are model parameters for the rough contact model as described in Zheng et al. (2021)

The radius expansion method (REM) was used to fill the chamber resulting in a porosity of 0.40 (void ratio of 0.67). Then, gravity was applied to settle the soil mass until reaching a state of equilibrium. During gravity settlement, the inter-particle friction coefficient was temporarily reduced to a relatively small value of 0.05 to attain a uniform and dense specimen. After equilibrium, the inter-particle friction coefficient was reset to the calibrated value (Table 1). All the chamber walls were fixed throughout simulations to create an unconfined condition.

Inspired by razor clam locomotion strategies, we modeled a dual-anchor probe to carry out the self-burrowing simulations. Geometrical details of the probe are shown in Figure 1c and Table 2. The probe was composed of three interconnected segments: shaft, neck and tip. The tip contains a cylinder that can expand to model as an anchor and a cone with the apex angle of 60°. The neck connects the tip cylinder and the embedment that extends to the end of the shaft. To prevent particles from flowing into the probe, each probe segment was created with end caps whose diameter also changes as the sections are expanded during anchor deployment.

Table 2. Geometrical properties of the chamber and the probe

Variable (unit)	Symbol	Value
Chamber height (cm)	H_C	70
Chamber diameter (cm)	D_C	70
Unscaled F-sand mean size (mm)	D_{50}	0.21
Number of particles	N	104,320
Probe total length (cm)	l_p	24.4
Probe material density (kg/m ³)	$ ho_p$	8,050
Chamber / probe diameter ratio	$D_C / D_T = R_d$	20
Probe / particle ratio in the core	$D_T / n_I D_{50} = n_p$	4.8

The probe-to-particle ratio n_p and chamber-to-probe diameter ratio R_d are two key factors to achieve sound soil penetration results. In this study, the final n_p in the central portion of the specimen is 4.8 and the R_d is 20, in accordance with previous simulations (Arroyo et al., 2011; Chen et al., 2021; Zhang et al., 2019). The contact model that describes the probe-particle interactions was also the simplified Hertz-Mindlin model (Table 1).

SELF-BURROWING SIMULATIONS

A stepwise self-burrowing methodology was designed closely following the locomotion strategy of razor clams. As illustrated in Figure 2, a single self-burrowing cycle of the probe was completed in six individual steps as follows:

- I. Shaft Expansion (SE): To deploy the shaft anchor, the shaft expanded radially under constant load control to reach a target force. A load control algorithm allows realistic interaction between the probe and soil. The expansion aims to provide sufficient reaction force for tip penetration in step B.
- II. Tip Penetration (TP): With the reaction of the shaft anchor, the neck and tip are moved downwards for a distance of $\Delta \rho_{tip}$ with a constant rate of 0.05 m/s. The stage is performed as long as the maximum sliding anchorage force, which is assumed to be determined from the radial shaft force $F_{S,r}$ multiplied by probe friction coefficient μ_p , remains greater than the total tip penetration resistance Q_T and the distance does not exceed the cone diameter. In this manner, the balance between the actual vertical anchorage force, which remains lower than its possible maximum value, and the soil resisting force is satisfied.
- III. Tip Expansion (TE): The tip cylinder is expanded to form the bottom anchor using a load control algorithm. The conical portion of the tip is not expanded to avoid interactions with the shaft anchor. The expansion aims to achieve a given target radial force.
- IV. Shaft Contraction (SC): The shaft is contracted to its original diameter at a constant rate of 0.1 m/s.
- V. Shaft Retraction (SR): The shaft is dragged downwards at a constant rate of 0.1 m/s until the shaft penetration distance $\Delta \rho_{shaft}$ is equal to $\Delta \rho_{tip}$. At this point, the original probe length returns to its original value. This stage is performed under the condition that the anchorage force of the tip is greater than the shaft retraction resistance.
- VI. Tip Contraction (TC): The tip was contracted back to its original size at a constant rate of 0.1 m/s.

Tip penetration. Among the self-burrowing steps, the most important and also challenging step is tip penetration because the essential motivation of developing this device is to burrow deeper into the soil. Hence, inspired by Polychaeta (Ortiz et al., 2019), we introduced a tip oscillation motion during penetration (Step B) to reduce the penetration resistance to improve the penetration efficiency. The oscillation algorithm is illustrated in Figure 3. The tip can oscillate horizontally in a vertical plane with a velocity of Vel_TO in one oscillation cycle time t_I . The amplitude $(0.25 \times Vel_TO \times t_I)$ and frequency $(1/t_I)$ of the oscillation are controlling parameters that can be adjusted to optimize tip penetration. We tried various sets of parameters combining different values of Vel_TO and t_I . Eventually, t_I =0.1 s and Vel_TO = 0.8 m/s were chosen for this study due to their efficient performance in enabling tip advance. The shaft radial force was maintained constant through Step B to enable enough penetration. Note that only vertical forces acting on the probe were checked as described previously, while the torque balance resulting from tip oscillation was not considered for simplicity.

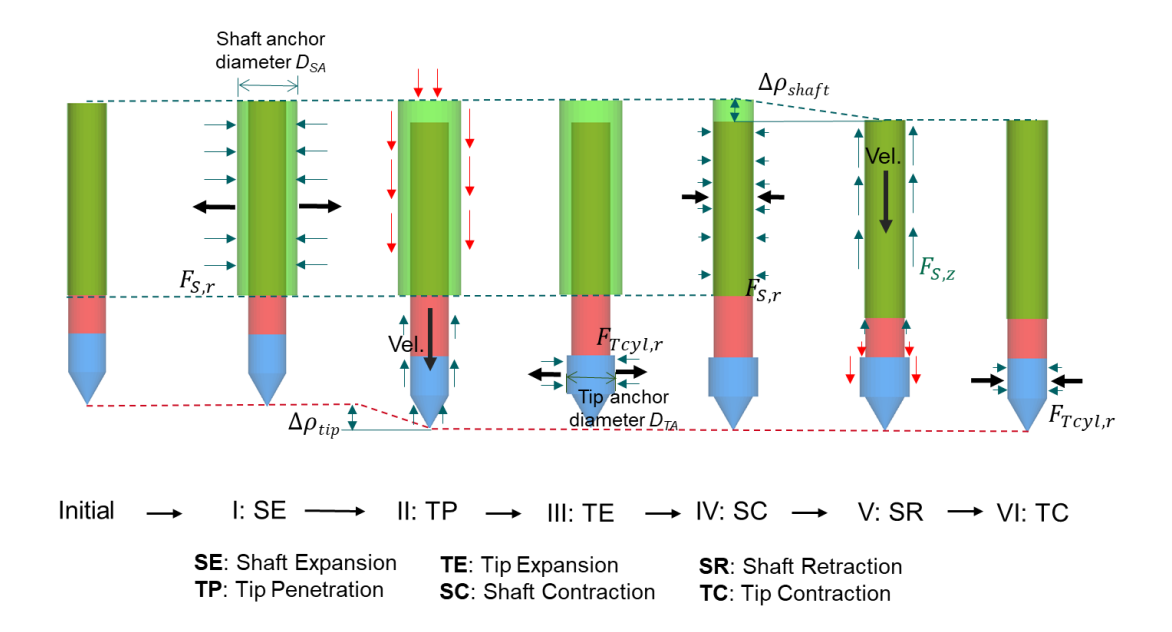


Figure 2. Illustration of a stepwise self-burrowing cycle. Thick black arrows indicate movement direction of one specific segment. Light blue arrows indicate direction of concerned forces.

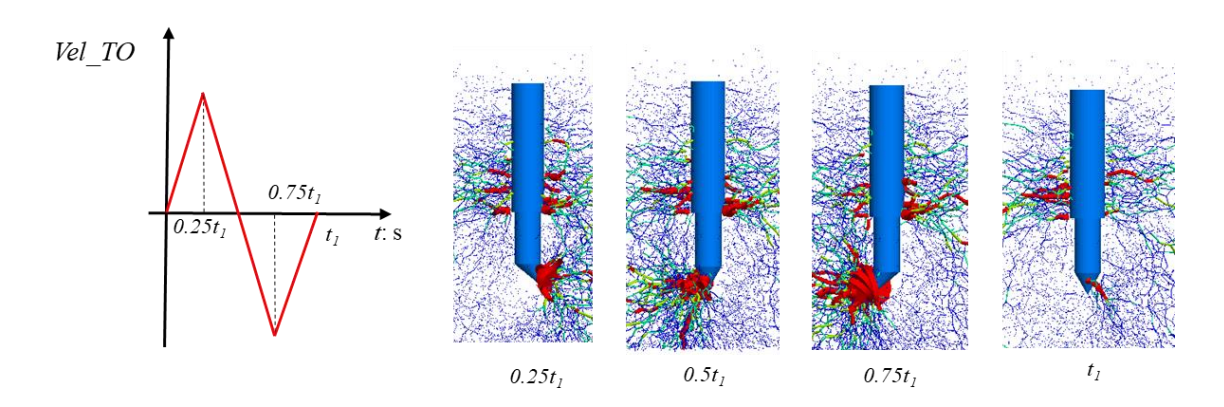


Figure 3. Illustration of tip oscillation algorithm adopted during tip penetration and contact force distribution observed at each characteristic time point.

RESULTS

Self-burrowing performance. To initiate the simulation, the probe was first pushed into the soil with a constant rate until the tip reached a depth of 34 cm, at which the entire probe was fully surrounded by soil particles that enabled the mobilization of enough anchorage force. Then a complete self-burrowing cycle was performed. Figure 4a shows the evolution of shaft and tip displacement measured during one complete self-burrowing cycle. With the implementation of tip oscillation, the tip could eventually burrow through a distance of 2 cm using a back anchor expanded to 50% of its initial radius, which was set as one stopping criterion of tip penetration. As demonstrated by the shaft displacement curve, the 2 cm displacement was quickly recovered

through shaft retraction. With the motivation of the satisfactory performance of the self-burrowing probe, multiple cycles are to be run to achieve deeper penetration in future studies.

Figure 4b shows the evolution of three representative probe force variables: tip resisting force Q_T , shaft radial force $F_{S,r}$, and radial force at the expanded tip cylinder $F_{Tcyl,r}$. The shaft anchorage force $(F_{S,r} * \mu_p)$ is greater than Q_T throughout the penetration, showing the sufficiency of the shaft anchor capacity. Significant interactions between the two radial forces $F_{S,r}$ and $F_{Tcyl,r}$ can be observed throughout the burrowing cycle. Interactive effects in SE and TP are not highly noticeable due to the employed controlling algorithm. However, the following interaction take place:

- TE. When tip expands, the shaft radial force $F_{S,r}$ decreases dramatically.
- SC. When the shaft contracts, $F_{S,r}$ drops to near 0, causing $F_{Tcyl,r}$ to reduce significantly.

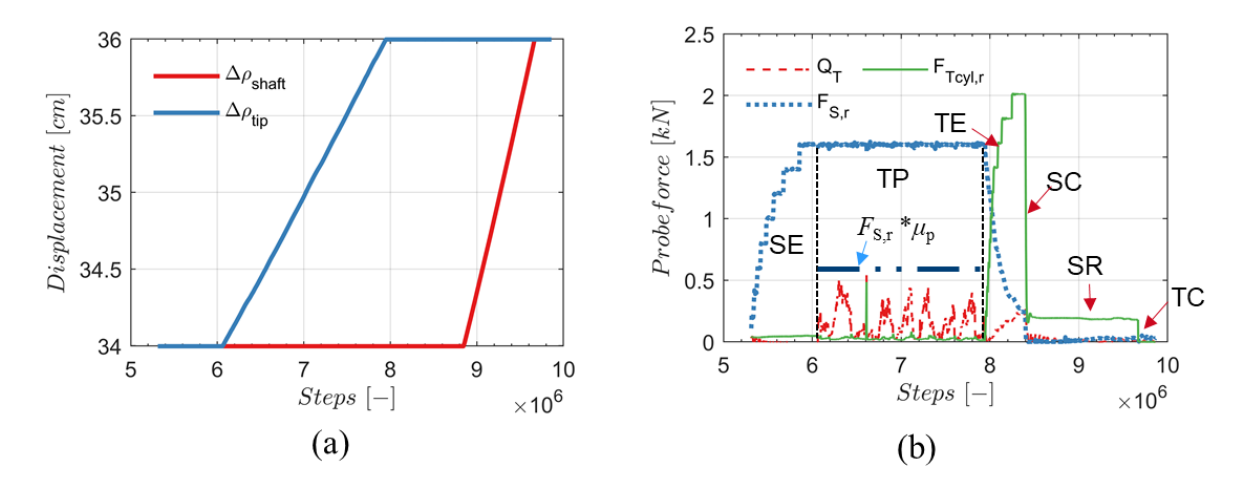


Figure 4. Self-burrowing performance: (a) burrowing displacement, and (b) characteristic forces recorded on probe segments.

Microscale observations. Figure 5 shows the development of both contact force network and displacement field at the end of steps A-F. The left and right side of each image present contact force magnitudes and particle displacement, respectively. The presented particle displacements are accumulated from the beginning of the first step in the self-burrowing cycle (step A) and only displacements above a value of 0.1 mm are shown in the images. These images present important micromechanical observations in each step:

- I: SE. The contact force is mainly concentrated at the shaft, particularly at its bottom due to the gravity-induced stress gradient and uniform expansion of the shaft. The uniform shaft expansion can be reflected from the relatively uniform distribution of particle displacement along the shaft.
- II: TP. At this step, the tip advances more deeply into the soil with the help of the tip oscillations and the maintenance of the shaft radial force. To maintain the shaft force, the shaft expands continuously with a relatively low expansion rate, leading to a more uniform distribution of contact forces and greater particle displacements along the shaft.
- III: TE. With tip expansion, the concentration of contact forces shifts locations from the shaft to the tip. The contact forces along the shaft becomes less notable compared with the previous steps. Correspondingly, the particles around the tip anchor displace radially as the target anchorage force is mobilized.

- IV: SC. The shaft contraction leads to an obvious decrease of the contact forces around the shaft and tip. The magnitudes of particle displacements decrease.
- V: SR. During shaft retraction, contact force concentration appears at the bottom of the shaft and there is no clear change of the contact forces around the tip.
- VI: TC. After tip contraction, the contact force network shows small magnitudes along the entire probe length, indicating a loosening effect of the self-burrowing behaviors.

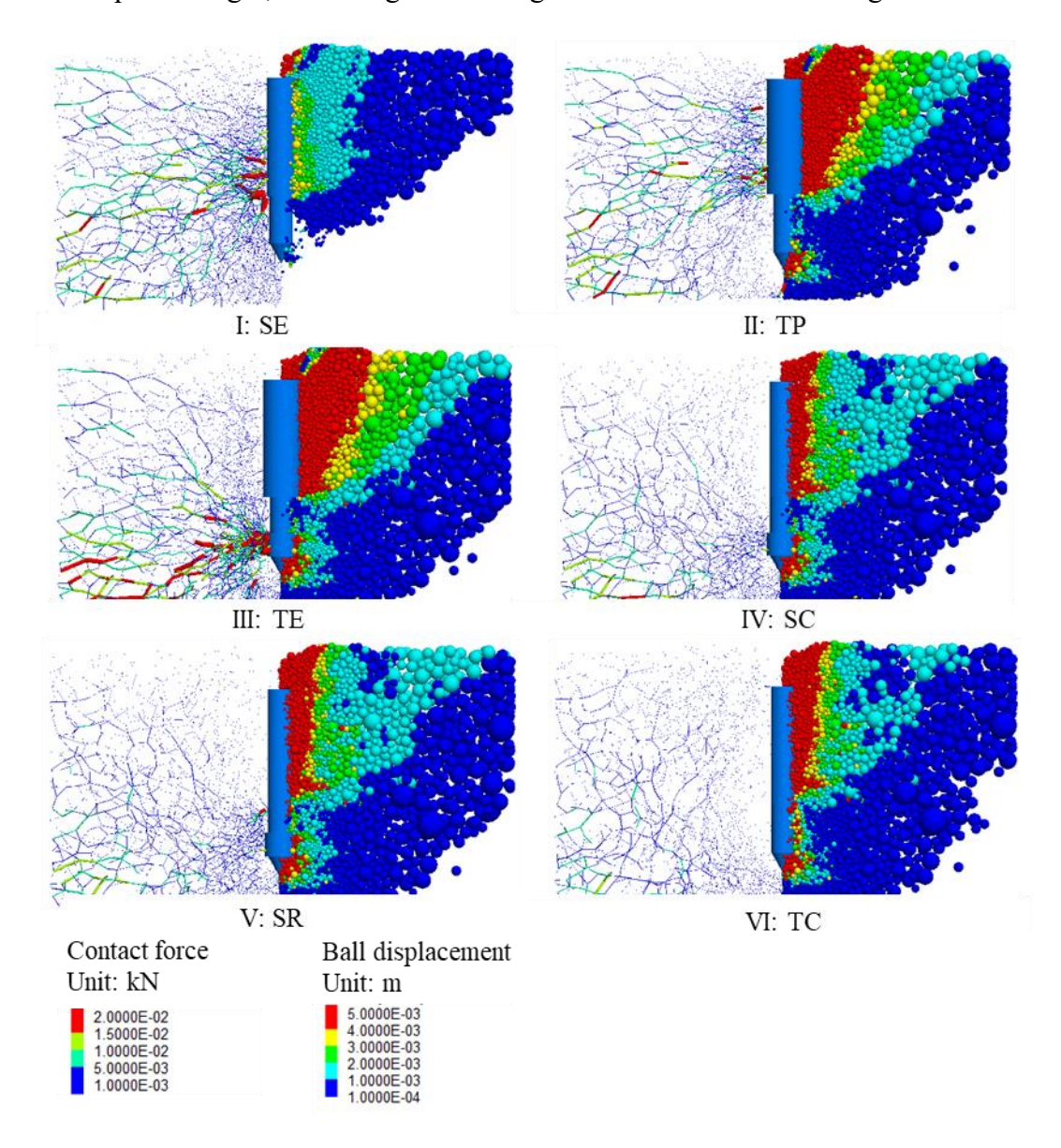


Figure 5. Micromechanical observations in each self-burrowing step. Left half of each image presents contact force and right half presents displacement.

CONCLUSIONS

In this paper we present DEM simulations of a bio-inspired self-burrowing probe in a chamber filled with a coarse-grained soil. A rough contact model has been used to more

realistically consider the sand mechanical behavior whose contact model parameters have been calibrated to model the behavior of silica sand. The simulated self-burrowing cycle consists of six individual steps including shaft expansion, tip penetration, tip expansion, shaft contraction, shaft retraction, and tip contraction. Among the steps, tip penetration is the most challenging due to the soil penetration resistance. Tip oscillation is employed to reduce the penetration resistance, which is proved to be an efficient strategy for enabling self-penetration. Significant interactions between the forces measured at the shaft and tip of the probe have been observed during tip expansion and shaft contraction. Microscale variables such as displacement and contact forces provide insightful particle-scale observations during a self-burrowing cycle. The satisfactory performance of a self-burrowing probe is expected to be tested in multiple cycles and samples with different soil conditions such as varying density levels.

ACKNOWLEDGEMENTS

This material is based upon work supported in part by the Engineering Research Center Program of the National Science Foundation under NSF Cooperative Agreement No. EEC–1449501. The second and third authors were supported in party by the National Science Foundation under Award No. 1942369. Any opinions, findings, and conclusions or recommendations expressed in this material are those of the author(s) and do not necessarily reflect those of the National Science Foundation.

REFERENCES

- Arroyo, M., Butlanska, J., Gens, A., Calvetti, F., and Jamiolkowski, M. (2011). Cone penetration tests in a virtual calibration chamber. *Géotechnique*, 61(6), 525–531.
- Chen, Y., Khosravi, A., Martinez, A., and Dejong, J. (2021). Modeling the self-penetration process of a bio-inspired probe in granular soils. *Bioinspiration and Biomimetics*, 16(4), 46012.
- Ciantia, M. O., Boschi, K., Shire, T., and Emam, S. (2018). Numerical techniques for fast DEM large-scale model generation. *Engineering and Computational Mechanics*.
- Huang, S., and Tao, J. (2020). Modeling Clam-inspired Burrowing in Dry Sand using Cavity Expansion Theory and DEM. *Acta Geotechnica*.
- Itasca, C. G. I. (2017). PFC Particle Flow Code, Ver. 5.0. Minneapolis.
- Martinez, A., Dejong, J. T., Jaeger, R. A., and Khosravi, A. (2020). Evaluation of self-penetration potential of a bio-inspired site characterization probe by cavity expansion analysis. *Canadian Geotechnical Journal*, 57(5), 706–716.
- Martinez, A., DeJong, J., Akin, I., Aleali, A., Arson, C., Atkinson, J., and Zheng, J. (2021). Bioinspired Geotechnical Engineering: Principles, Current Work, Opportunities and Challenges. *Géotechnique*, 1–48.
- McDowell, G. R., Falagush, O., and Yu, H. S. (2012). A particle refinement method for simulating DEM of cone penetration testing in granular materials. *Geotechnique Letters*, 2(7–9), 141–147.
- Ortiz, D., Gravish, N., and Tolley, M. T. (2019). Soft Robot Actuation Strategies for Locomotion in Granular Substrates. *IEEE Robotics and Automation Letters*, 4(3), 2630–2636.
- Sharif, Y., Brown, M., Cerfontaine, B., Davidson, C., Ciantia, M., Knappett, J., and Ottolini, M. (2020). Effects of screw pile installation on installation requirements and in-service performance using the Discrete Element Method. *Canadian Geotechnical Journal*.

- Ting, J. M., Corkum, B. T., Kauffman, C. R., and Greco, C. (1989). Discrete numerical model for soil mechanics. *Journal of Geotechnical Engineering*, 115(3), 769–787.
- Trueman, E. R. (1967). The dynamics of burrowing in Ensis (Bibalvia). In Proceedings of the Royal Society of London. Series B, Containing papers of a Biological character. *Royal Society (Great Britain)* (Vol. 166, pp. 459–476).
- Winter, V., Deits, R. L. H., Dorsch, D. S., Slocum, A. H., and Hosoi, A. E. (2014). Razor clam to RoboClam: Burrowing drag reduction mechanisms and their robotic adaptation. *Bioinspiration and Biomimetics*, 9(3).
- Zhang, N., Arroyo, M., Ciantia, M. O., Gens, A., and Butlanska, J. (2019). Standard penetration testing in a virtual calibration chamber. *Computers and Geotechnics*, 111(3), 277–289.
- Zhang, N., Ciantia, M. O., Arroyo, M., and Gens, A. (2021). A contact model for rough crushable sand. *Soils and Foundations*, (xxxx).